https://doi.org/10.15407/knit2024.04.003
UDC 629.78

A. ALPATOV[1,2] Corresponding Member of the National Academy of Sciences of Ukraine, Full-professor, Doctor of Engineering, Head of the Department of System Analysis and Control Problems,
ORCID: https://orcid.org/0000-0003-4411-2250
E-mail: aalpatov@ukr.net
C. WANG[2], Ph. D., Professor
ORCID: https://orcid.org/0000-0002-1358-7731
E-mail: wangcq@nwpu.edu.cn
H. LU[2,3], Ph. D., Postdoctoral
ORCID: https://orcid.org/0000-0003-4695-3424
E-mail: luhs@nwpu.edu.cn
E. LAPKHANOV[1], Ph. D., Researcher at the Department of System Analysis and Control Problems
ORCID: https://orcid.org/0000-0003-3821-9254
E-mail: ericksaavedralim@gmail.com

[1] Institute of Technical Mechanics of the National Academy of Sciences of Ukraine and the State Space Agency of Ukraine
5 Leshko-Popel Str., Dnipro, 49005 Ukraine
[2] School of Automation, Northwestern Polytechnical University
Xi'an, China
[3] Chongqing Innovation Center, Northwestern Polytechnical University
Chongqing, China

ORBIT SELECTION OF THE SPACE INDUSTRIAL PLATFORM WITH DISTRIBUTED ELECTRICAL-POWER SYSTEM MODULES

Space industrialization is one of the prospective directions in modern aerospace science and engineering for space exploration of new resources and habitats. The key issue is to provide industrial space modules with the required amount of electricity needed. One type of power supply for such modules is the use of distributed power systems, which consist of constellations of spacecraft with contactless power transmission. Given this, the problem of rational orbit selection for their dislocation arises. Considering these problems, the methodology for orbits selection of the space industrial platform with distributed electrical-power system modules is proposed in the paper. This methodology includes orbital translation, attitude, relative dynamics estimation for each power satellite, and its corresponding orbit optimization algorithm. The orbit optimization algorithm includes statistical processing and elements of gradient and coordinate descent methods, allowing us to determine the most significant parameter influencing the duration of the contactless power transmission session. Also, quaternion mathematics is used to estimate the dynamics in the program parameters for targeting the transmitter spacecraft antenna to the receiver spacecraft rectenna. With the approaches mentioned above, the methodology proposed in this paper allows us to form the requirements for the power satellites' attitude and orbit control system to improve the process of selecting corresponding design parameters of such systems.

Thus, the usage of the proposed methodology can allow the designing of the power satellites' attitude and orbit control system in the conceptual stages of designing.

Keywords: *contactless power transmitting, orbit selection, targeting quaternion, optimization of orbit parameters.*

Цитування: Alpatov A., Wang C., Lu H., Lapkhanov E. Orbit selection of the space industrial platform with distributed electrical-power system modules. *Space Science and Technology.* 2024. **30**, No. 4 (149). P. 03—23. https://doi.org/10.15407/knit2024.04.003

Introduction. The Near Future requires New Future Ideas and Technical Propositions. One of these new ideas is connected with the concept of Space Industrialization. The development of the Space Industrialization Concept has grown based on two main scientific directions, which are the study of large space constructions and space manufacturing research. Given this, the leading world space agencies have proposed several technical approaches that allow one to produce unique technologies in zero gravity. These technologies are connected with production semiconductors, space inductive metallurgy, 3D printing technologies, etc.

In turn, implementation of such power-consuming technological processes requires significant onboard electrical power reserves on the space industrial platform. Taking this into account, there is a task of the development of a space industrial platform electrical power system. This system should consist of four main modules:

1) the electricity generation module;

2) the electricity storage module;

3) the module for transmitting electricity to a consumer (Space industrial platform equipment);

4) the module for receiving and converting electricity.

Considering the level of theoretical and practical background of solar power satellite development [7, 12, 15], the power-electrical system of the space industrial platform can be constructed using two approaches. The first approach is based on placing all 4 electrical-power structural modules on the one bus platform together with all systems of the space industrial platform (SIP). However, such an approach requires a significant area for solar panels' placement and free volume for the batteries' location. This reduces the free volume inside the SIP, which is necessary for placing technical industrial equipment. On this basis, the problem of selecting a rational ratio of production equipment mass to the electrical-power system mass arises. Given the limitation of the volume inside the SIP and the reduction of free volume for useful equipment due to the installation of energy modules, the efficiency of the SIP itself can be significantly reduced.

Therefore, in [20], the second approach has been proposed based on the distribution of electrical-power modules between the SIP bus and the special electrical-power spacecraft orbital group (SEPSOG). Such configuration can allow us to reduce the free volume inside SIP, which is required for the power generation system in the first case. Considering this, the task of ballistic analysis for orbital, attitude, and relative motion of SEPSOG modules arises.

Literature review and problem statement. Research on space power systems (SPS) has been carried out by the Japan Aerospace Exploration Agency (JAXA) since the early 2000s. The research group of the JAXA presented a phased program for the creation of a commercial SPS [23]. The configuration of the space-based solar power system consists of numerous square panels, each measuring 100 m × 95 m and 0.1 m thick, tethered together. Each panel is suspended at the corners on 4 cables 5—10 km long, coming out from the bus system. The mass of a single system, according to [23], is about 50 tons, and the power transmitting capability is 2.2 MW. Moreover, this technology was tested in space. However, this approach has several disadvantages when using such SPS as SEPSOG modules for SIP. These disadvantages are:

1) usage of the large construction leads to reducing the maneuvering performance during guidance and re-orientation;

2) probability of additional vibrations and oscillations in the articulated joints [14], which leads to additional disturbances in reorientation modes and reduces the pointing accuracy;

3) problems of providing accurate orientation in tracking modes of targeting on the apertures of SIP receivers.

These disadvantages and problems can occur when using all types of super-large space constructions [18] for contactless electricity transmission between two spacecraft. Even though good results have been obtained in the Earth-pointing accuracy of the large-sized space power plant transmitting antenna [17], such systems are very difficult to apply in the SEPSOG technologies. It can be explained by the two peculiarities of large-scale SPS concept implementation:

- the large-scale SPS technologies are proposed to be located on Geosynchronous orbits with constant relative position to the target point of the receiver, which is located on the Earth's surface,

• lack of target tracking modes and moving receivers that require high performance and accuracy for the attitude and orbit control subsystem (AOCS), which are needed for SEPSOG modules.

Therefore, the peculiarities of SEPSOG module construction should take into account all of the above-mentioned shortcomings. In turn, further research shows the possibility of reducing the mass and dimensions of SPS [25]. So, according to estimation, the total mass of SPS was proposed to be near 2000 kg. The area of solar panels is about 141 m^2, which significantly impacts the inertial characteristics of this power satellite [25]. However, this satellite is developed for the power transition to the terrestrial receivers from orbit altitudes ranging from 8500 to 16500 km. Given the much smaller distance between the SIP receivers and the SEPSOG transmitting satellites, the energy loss will also be much less. Therefore, the development of SEPSOG will not require such a large power generation system and such a large area of solar panels, as has been proposed in [25]. In turn, it can help us significantly reduce the elastic perturbations in the articulated joints, which have an oscillation nature.

The method of reducing oscillation impact for SPS is proposed in the paper [24]. This method assumes the control law for a micro-electromechanical system, which allows us to suppress vibrations for SPS during on-orbit assembly. However, implementation of such an approach requires a lot of additional sensors, actuators, and control modules, which can significantly increase the costs for the creation of such SPS. On the other hand, nothing is clear about the operation of such a control system in the target tracking modes that are required for SEPSOG modules.

Taking this into account, the mechanical body construction of the SEPSOG module should have properties that are close to rigid body dynamics when elastic oscillation will be minimal and can be neglected.

The closest concept to the SEPSOG is described in works [1, 5]. This approach is based on the contactless microwave power transition between two satellites. So, it has been shown the possibility of wireless power transition between two microsatellites (Figure 1), which are:

1) transmitting microsatellite with a mass of 50 kg [4],

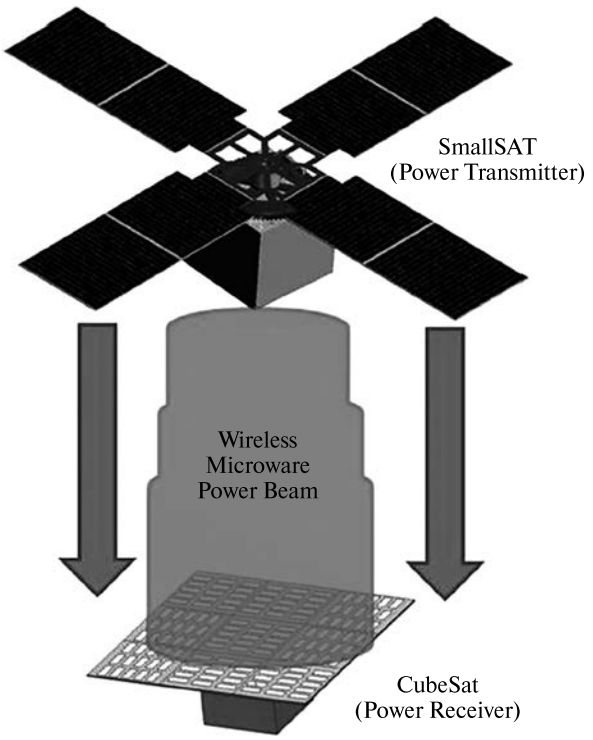

Figure 1. Microwave wireless power transmitting between two satellites

2) receiving satellite with a mass of 1.33 kg (CubeSat class) [4].

According to the estimations [5], the possible transmitting distance between these two satellites ranges from 8 to 300 m depending on the wavelength (which depends on the operating frequency of the microwave range) and antenna/rectenna sizes. Taking this into account, for such types of satellites, only one type of flight is possible during power transmission — a formation flight with maintaining a constant distance between satellites. In turn, according to the analysis, which has been done in the paper [1], the most expedient method of power transition is based on microwave power transition. It can be explained by the deep study of this technology and experimental verification and confirmation of the theoretical calculation of contactless power transmission. However, laser contactless power transition is in progress and, according to the authors' suggestions, has good perspectives in the future [1].

Considering all the above peculiarities of contactless power transmission between two satellites in

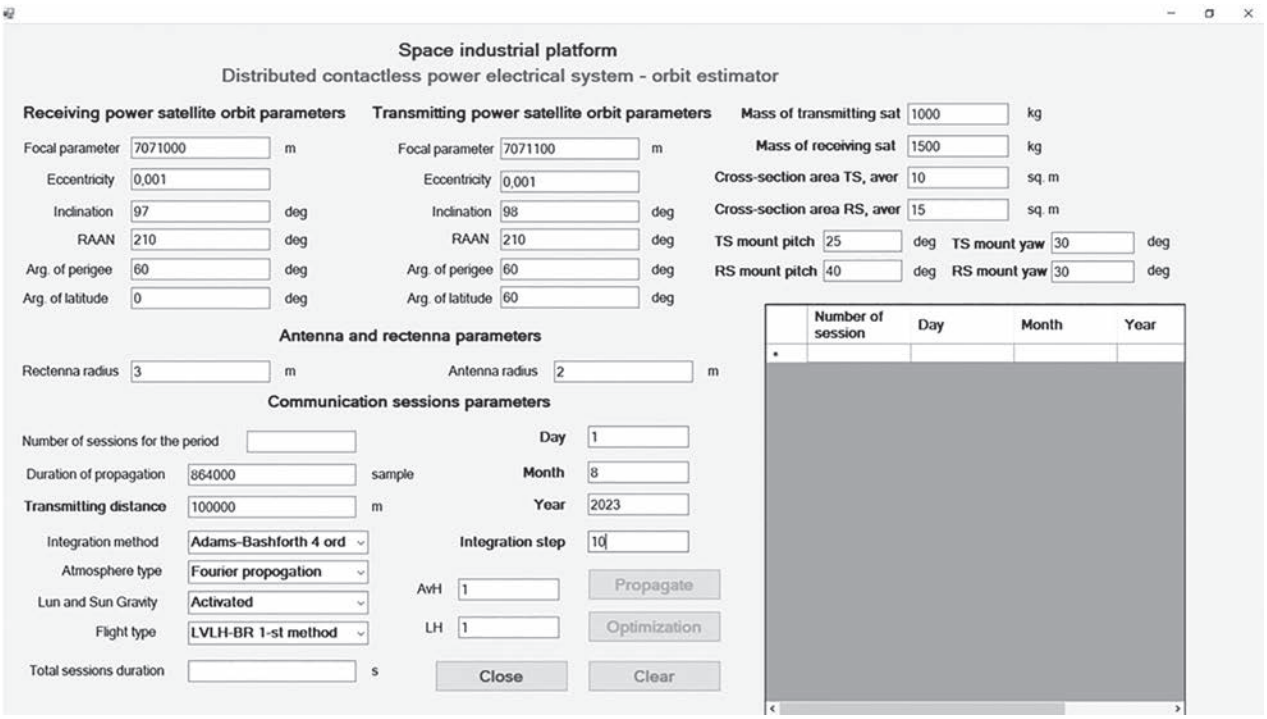

Figure 2. The main window of the GUI interface

space, the following tasks, which should be solved to determine SEPSOG dislocation, can be defined:

1) determination of SIP orbit parameters [20],

2) determination of SEPSOG orbits [20],

3) analysis of relative motion: SEPSOG modules relative to SIP,

4) determination of the distance changes between SEPSOG modules and SIP during orbiting [20],

5) determination of the conditions that allow contactless power transmission from the SEPSOG module to SIP receivers.

Taking into account the listed problems, the task arises of developing the methodology for SEPSOG orbiting analysis and determining their dislocations.

The purpose and tasks of the study. The **purpose** of the research is to develop the methodology for SEPSOG orbits' selection while considering the space industrial platform position. This will make it possible to choose the orbit locations for SEPSOG modules of the space-based distributed power system of the space industrial platform considering the requirements of contactless power transition.

To achieve this aim, it has been determined a set of following tasks:

– to determine the mathematical model of SEPSOG orbital translation and relative motion,

– to develop the mathematical model for targeting quaternion (quaternion of SEPSOG transmitting spacecraft orientation to SEPSOG receiving spacecraft aperture) estimation,

– to carry out a numerical experiment on the choice of the location of the SEPSOG modules,

– to develop the methodology for determining the most optimal orbital parameters for the location of the SEPSOG modules.

Materials and methods of research. The object of the research is the process of determining spacecraft ballistic parameters by analyzing the orbital group's relative motion. The subject of the research is the theoretical and conceptual aspects of the methodology development using orbital mechanics theory, theory of optimization, and computer simulation for the orbit selection of spacecraft of the space industrial platform electrical-power distributed system.

To solve the problems presented in the study, we employed general scientific and specialized research methods:

– methods of celestial mechanics and spacecraft flight theory for determination of SEPSOG ballistic parameters,

– methods of mathematical analysis, vector algebra, numerical simulation, and quaternion mathematics for the development of a mathematical model of SEPSOG motion,

– methods of software development for the creation of software GUI module using the multilanguage approach,

– method of system analysis.

To study the peculiarities of the motion of the SEPSOG modules, a special software application has been developed. Structurally, this application consists of 3 parts:

1) dll library, which includes mathematical models for the SEPSOG orbital motion simulation (developed using C++),

2) general algorithm and programs for library integration to software application (developed on C#),

3) GUI interface and file system (developed on C#).

In turn, the main window of the GUI interface (Figure 2) allows one to input main SEPSOG parameters, including orbits, mass, and size, apertures sizes, and space environment parameters to analyze the relative motion of two SEPSOG modules: spacecraft transmitter (SCT) and spacecraft receiver (SCR). Also, this window includes a database table, which records the duration of possible sessions of contactless power transmission from SCT to SCR.

The additional window of the GUI interface is developed for the graphical visualization of calculations.

Mathematical model of special electrical-power spacecraft group orbital translation and relative motion. The generalized mathematical model of SEPSOG motion is described in [20]. This mathematical model includes:

1) 6-dof model of spacecraft perturbative motion,

2) module for SCT and SCR relative motion determination,

3) general mathematical approaches for the targeting subsystem development,

4) general approaches for AOCS control algorithm development,

5) a general description of the requirements for contactless power transmission from SCT to SCR.

In turn, the following mathematical models, which are used in the dll library of the software application, include:

***A*)** 3-dof model of spacecraft perturbative translation motion based on the differential equations in orbital parameters [20, 22]. For the correct implementation of this mathematical model, the following standard reference frames were used, which are described in [2, 9, 10, 20]. These reference frames are the J2000 inertial reference frame [20], WGS-84 reference frame [9], STW orbital reference frame [10], local vertical local horizontal (LVLH) reference frame, SCR and SCT body and aperture reference frames (ARF) [20]. In turn, the differential equation model has the following form:

$$\left.\begin{aligned}
&\frac{d\Omega}{dt}=\frac{r_{SC}}{\sqrt{\mu\cdot p}}\cdot\frac{\sin u}{\sin i}\cdot W\\
&\frac{di}{dt}=\frac{r_{SC}}{\sqrt{\mu\cdot p}}\cdot\cos u\cdot W\\
&\frac{dp}{dt}=2r_{SC}\cdot\sqrt{\frac{p}{\mu}}\cdot T\\
&\frac{dq}{dt}=\sqrt{\frac{p}{\mu}}\left[\sin u\cdot S+\left(\left(1+\frac{r_{SC}}{p}\right)\cos u+\frac{r_{SC}}{p}q\right)T+\right.\\
&\left.+\frac{r_{SC}}{p}k\sin u\cdot\cot i\cdot W\right]\\
&\frac{dk}{dt}=\sqrt{\frac{p}{\mu}}\left[-\cos u\cdot S+\left(\left(1+\frac{r_{SC}}{p}\right)\sin u+\frac{r_{SC}}{p}k\right)T-\right.\\
&\left.-\frac{r_{SC}}{p}q\sin u\cdot\cot i\cdot W\right]\\
&\frac{du}{dt}=\frac{\sqrt{\mu p}}{r_{SC}^2}\left(1-\frac{r_{SC}^3}{\mu p}\cot i\cdot\sin u\cdot W\right)
\end{aligned}\right\},\qquad(1)$$

where

$$r_{SC}=\frac{p}{1+q\cos u+k\sin u}$$

is the module of the spacecraft radius-vector (distance from the Earth's center to the spacecraft),

$$\omega=\arctan\left(\frac{k}{q}\right),\ q=e\cos\omega,\ k=e\sin\omega.$$

are the components of the Laplace vector, a is the orbit semi-major axis, e is the eccentricity of the orbit, Ω is the RAAN of the orbit, ω is the argument of perigee, μ is the gravity constant, $\mu = 3.986 \cdot 10^5$ km^3/s^2; p is the focal parameter of the orbit, $p = a\left(1-e^2\right)$, i is the inclination of the orbit, u is the orbit argument of latitude, ϑ is the orbit truth anomaly, t is the time of spacecraft motion, S,T,W are projections of the disturbing radial, transversal, and normal accelerations on the axis of the STW reference frame.

The following perturbative components of *S, T, W* accelerations are taken into account in the 3-dof model:

1) Gravitational perturbations. Gravitational perturbations are represented by a decomposition of the Earth's gravitational potential by spherical functions in the form of Legendre polynomials. Zonal, tesseral, and sectoral harmonics up to order 10, including Earth's precession and nutation, are taken into account. The model of gravitational field is presented in [19, 26].

2) Aerodynamic perturbations. The aerodynamic perturbations are calculated according to the methodology in [9].

3) Solar pressure perturbations. The perturbations from the impact of solar pressure are calculated according to the methodology in [9].

4) Lunar and solar gravitational perturbations are calculated according to the methodology described in [19].

B) Calculation of the kinematic parameters of SCT and SCR in the J2000 reference frame:

– the vectors of SCR and SCT positions ($\mathbf{R_{SCR}}$ and $\mathbf{R_{SCT}}$),

– the vectors of SCR and SCT orbital velocity ($\mathbf{V_{SCR}}$ and $\mathbf{V_{SCT}}$).

These vectors depend on the orbital parameters of SCT and SCR [20], which are calculated according to the model (1). In turn, $\mathbf{R_{SCR}}$, $\mathbf{R_{SCT}}$, $\mathbf{V_{SCR}}$, $\mathbf{V_{SCT}}$ are calculated from orbital parameters according to the formulas which are presented in [20].

C) Estimation of the SCT and SCR relative motion parameters:

– the current relative distance between SCT and SCR, R_{rel},

– current absolute value of relative velocity between SCT and SCR, V_{rel}.

The R_{rel} and V_{rel} are calculated using the following formulas [20]:

$$R_{rel} = \sqrt{\left(R_{SCT.X} - R_{SCR.X}\right)^2 + \left(R_{SCT.Y} - R_{SCR.Y}\right)^2 + \left(R_{SCT.Z} - R_{SCR.Z}\right)^2},$$

$$V_{rel} = \sqrt{\left(V_{SCT.X} - V_{SCR.X}\right)^2 + \left(V_{SCT.Y} - V_{SCR.Y}\right)^2 + \left(V_{SCT.Z} - V_{SCR.Z}\right)^2}, \quad (2)$$

where $R_{SCT.X}$, $R_{SCT.Y}$, $R_{SCT.Z}$ are the components of vector $\mathbf{R_{SCT}}$; $R_{SCR.X}$, $R_{SCR.Y}$, $R_{SCR.Z}$ are the components of vector $\mathbf{R_{SCR}}$; $V_{SCT.X}$, $V_{SCT.Y}$, $V_{SCT.Z}$ are the components of vector $\mathbf{V_{SCT}}$; $V_{SCR.X}$, $V_{SCR.Y}$, $V_{SCR.Z}$ are the components of vector $\mathbf{V_{SCR}}$.

D) Determination of the connection session time. The number of connection sessions and their durations are calculated taking into account the following condition:

$$R_{rel} \le D_{\max}, \quad (3)$$

where $D_{\max}$ is the maximal distance of contactless power transition between SCT and SCR.

In turn, $D_{\max}$ depends on SCT antenna parameters, SRT rectenna parameters, frequency of the power transition microwave and, according to [5], can be written as:

$$\tau = \frac{\sqrt{A_t A_r}}{\lambda D_{\max}}, \quad (4)$$

where τ is the dimensionless contactless power transfer coefficient between the antenna and rectenna, A_t is the area of the SCT transmitting antenna, A_r is the area of the SCR receiving antenna (rectenna), λ is the wavelength of the microwave power being transmitted.

Also, the estimation of power transition on the maximum distance between the antenna and rectenna can be done using the following formula [5]:

$$p_d = \frac{A_t P_t}{\lambda^2 D_{\max}^2}, \quad (5)$$

where p_d is the power density at the center of the SCR rectenna, P_t is the total radiated power from the SCT transmitter.

Considering the dependences in formulas (4) and (5), it can be concluded that the value of $D_{\max}$ fully

depends on the parameters of SCT and SCR microwave equipment. So, each power transmitting session time is calculated using the following **algorithm:**

***Step 1*)** Determination of initial SCT and SCR orbits.

***Step 2*)** Run the simulation of STR and SCR orbital motion using GUI software with an integrated .dll library, which includes an orbital motion propagator based on a mathematical model (1).

***Step 3*)** Calculation of STR and SCR relative motion parameters R_{rel} and V_{rel} (2) at each step of integration of differential equations (1).

***Step 4*)** Check the condition (3):

• *if condition* (3) is ***true,*** then save the current board time and start the session duration countdown;

• *if condition* (3) is **false,** then stop the session duration countdown and calculate the session duration.

Thus, these algorithms can be used to determine the number of communication sessions for a certain period of propagation of the SCT and SCR orbital motion and their duration. Another issue is determining the dynamics of changes in the angular targeting parameters (angles or/and quaternion) of the receiver and transmitter apertures during communication sessions. This will be necessary for selecting AOCS system parameters of SCT and SCR in the case of their development.

Mathematical model for targeting quaternion estimation. Considering estimated vectors $\mathbf{R_{SCT}}$, $\mathbf{V_{SCT}}$, $\mathbf{R_{SCR}}$, $\mathbf{V_{SCR}}$, it will be possible to calculate the targeting quaternions for SCR and SCT according to [20]. In turn, in paper [20], a general approach was proposed for determining angular kinematic parameters using quaternion calculation from roll, pitch, and yaw angles. This can lead to additional calculations and some singularities which can be observed in the case of roll, pitch, yaw angles calculation from a matrix. Considering this, the following algorithm for targeting quaternion determination has been proposed:

Using $\mathbf{R_{SCT}}$ and $\mathbf{V_{SCT}}$ vectors for SCT or $\mathbf{R_{SCR}}$ and $\mathbf{V_{SCR}}$ vectors for SCR to create a unit vector basis, use the following steps:

I) Normalize $\mathbf{R_{SCT}}$, $\mathbf{V_{SCT}}$, $\mathbf{R_{SCR}}$, $\mathbf{V_{SCR}}$ vectors, dividing each coordinate by the corresponding L-2 norm [20]. The corresponding unit vectors of $\mathbf{R_{SCT}}$, $\mathbf{V_{SCT}}$, $\mathbf{R_{SCR}}$, $\mathbf{V_{SCR}}$ are denoted as follows: $\mathbf{r_{SCT}}$, $\mathbf{v_{SCT}}$, $\mathbf{r_{SCR}}$, $\mathbf{v_{SCR}}$.

II) Determine the unit vector bases $O_R X_R Y_R Z_R$ / $O_T X_T Y_T Z_T$ for SCR and SCT using the properties of the Frenet–Serret trihedron and double cross product [3, 26]:

1) $O_R Z_R = -\mathbf{r_{SCR}}$, $O_T Z_T = -\mathbf{r_{SCT}}$,

2) $O_R Y_R = -\mathbf{r_{SCR}} \times \mathbf{v_{SCR}}$, $O_T Y_T = -\mathbf{r_{SCT}} \times \mathbf{v_{SCT}}$,

3) $O_R X_R = O_R Y_R \times O_R Z_R$, $O_T X_T = O_T Y_T \times O_T Z_T$.

These vector bases are needed for the determination of transiting matrices from J2000 to LVLH reference frame for SCR and SCT.

III) Determine transiting matrices from LVLH to J2000:

for SCR:

$$M^{SCR}_{LVLH\to J2000} = \left[\begin{array}{c|ccc} J & & \underline{L\quad V\quad L\quad H} & \\ 2 & O_R X_R.x & O_R Y_R.x & O_R Z_R.x \\ 0 & O_R X_R.y & O_R Y_R.y & O_R Z_R.y \\ 0 & O_R X_R.z & O_R Y_R.z & O_R Z_R.z \end{array}\right], \quad (6)$$

for SCT:

$$M^{SCT}_{LVLH\to J2000} = \left[\begin{array}{c|ccc} J & & \underline{L\quad V\quad L\quad H} & \\ 2 & O_T X_T.x & O_T Y_T.x & O_T Z_T.x \\ 0 & O_T X_T.y & O_T Y_T.y & O_T Z_T.y \\ 0 & O_T X_T.z & O_T Y_T.z & O_T Z_T.z \end{array}\right], \quad (7)$$

where $O_R X_R.x$, $O_R X_R.y$, $O_R X_R.z$ are the components of the unit vector $O_R X_R$; $O_R Y_R.x$, $O_R Y_R.y$, $O_R Y_R.z$ are the components of the unit vector $O_R Y_R$; $O_T Z_T.x$, $O_T Z_T.y$, $O_T Z_T.z$ are the components of the unit vector $O_R Z_R$; $O_T X_T.x$, $O_T X_T.y$, $O_T X_T.z$ are the components of the unit vector $O_T X_T$; $O_T Y_T.x$, $O_T Y_T.y$, $O_T Y_T.z$ are the components of the unit vector $O_T Y_T$; $O_T Z_T.x$, $O_T Z_T.y$, $O_T Z_T.z$ are the components of the unit vector $O_T Z_T$.

IV) Calculate the targeting vectors from SCR to SCT and from SCT to SCR:

$$\mathbf{R^{tar}_{SCT\to SCR}} = \begin{bmatrix} R_{SCR.X} - R_{SCT.X} \\ R_{SCR.Y} - R_{SCT.Y} \\ R_{SCR.Z} - R_{SCT.Z} \end{bmatrix}, \quad \mathbf{R^{tar}_{SCR\to SCT}} = \begin{bmatrix} R_{SCT.X} - R_{SCR.X} \\ R_{SCT.Y} - R_{SCR.Y} \\ R_{SCT.Z} - R_{SCR.Z} \end{bmatrix}, \quad (8)$$

where $R_{SCR.X}$, $R_{SCR.Y}$, $R_{SCR.Z}$ are the components of the vector $\mathbf{R_{SCR}}$, $R_{SCT.X}$, $R_{SCT.Y}$, $R_{SCT.Z}$ are the components of the vector $\mathbf{R_{SCT}}$.

V) Normalize the

$$\mathbf{R^{tar}_{SCT\to SCR}} \text{ and } \mathbf{R^{tar}_{SCR\to SCT}}$$

vectors dividing each coordinate by the corresponding L-2 norm. The corresponding unit vectors of

$$\mathbf{R^{tar}_{SCT\to SCR}} \text{ and } \mathbf{R^{tar}_{SCR\to SCT}}$$

are denoted as follows:

$$\mathbf{r^{tar}_{SCT\to SCR}} \text{ and } \mathbf{r^{tar}_{SCR\to SCT}}.$$

VI) Determination of the

$$\mathbf{r^{tar}_{SCT\to SCR}} \text{ and } \mathbf{r^{tar}_{SCR\to SCT}}$$

values in corresponding SCT and SCR LVLH reference frames using formulas (6) and (7). It can be written as:

$$\mathbf{r^{tar}_{SCT\to SCR.LVLH}} = \left(M^{SCT}_{LVLH\to J2000}\right)^{\mathrm{T}} \cdot \mathbf{r^{tar}_{SCT\to SCR}},$$

$$\mathbf{r^{tar}_{SCR\to SCT.LVLH}} = \left(M^{SCR}_{LVLH\to J2000}\right)^{\mathrm{T}} \cdot \mathbf{r^{tar}_{SCR\to SCT}}, \quad (9)$$

where

$\mathbf{r^{tar}_{SCT\to SCR.LVLH}}$ is the $\mathbf{r^{tar}_{SCT\to SCR}}$ vector

in LVLH reference frame,

$\mathbf{r^{tar}_{SCR\to SCT.LVLH}}$ is the $\mathbf{r^{tar}_{SCR\to SCT}}$ vector

in LVLH reference frame.

VII) Determination of the transiting matrices from LVLH to SCR and from LVLH to SCT body frames. Transiting matrices from LVLH to SCR and SCT body frames $O_{BR}X_{BR}Y_{BR}Z_{BR}$ / $O_{BT}X_{BT}Y_{BT}Z_{BT}$ can be found using algorithms, which are presented in [20]. In turn, it has been proposed to use the first algorithm [20] for the determination of transiting matrices. It can be written as follows:

1) set a special unit vector $\mathbf{u_n} = \begin{bmatrix} 0 & 0 & 1 \end{bmatrix}^T$;

2) assume that axes $O_{BR}X_{BR}$ and $O_{BT}X_{BT}$ coincide with $\mathbf{r^{tar}_{SCR\to SCT.LVLH}}$ and $\mathbf{r^{tar}_{SCT\to SCR.LVLH}}$ during SCR/SCT rotation relative to LVLH in target modes;

3) $O_{BR}Y_{BR} = \mathbf{u_n} \times \mathbf{r^{tar}_{SCR\to SCT.LVLH}}$,

$O_{BT}Y_{BT} = \mathbf{u_n} \times \mathbf{r^{tar}_{SCT\to SCR.LVLH}}$;

4) $O_{BR}Z_{BR} = -O_{BR}Y_{BR} \times O_{BR}X_{BR}$,

$O_{BT}Z_{BT} = -O_{BT}Y_{BT} \times O_{BT}X_{BT}$.

Using a similar algorithm as in (6) and (7), we determine the transiting matrices from LVLH to SCT body frame $M^{SCT}_{LVLH\to BODY}$ and from LVLH to SCR body frame $M^{SCR}_{LVLH\to BODY}$ as follows:

for SCR:

$$M^{SCR}_{LVLH\to BODY} = \left[\begin{array}{c|ccc} B & & \overline{L \quad V \quad L \quad H} & \\ O & O_{BR}X_{BR}.x & O_{BR}X_{BR}.y & O_{BR}X_{BR}.z \\ D & O_{BR}Y_{BR}.x & O_{BR}Y_{BR}.y & O_{BR}Y_{BR}.z \\ Y & O_{BR}Z_{BR}.x & O_{BR}Z_{BR}.y & O_{BR}Z_{BR}.z \end{array}\right], \quad (10)$$

for SCT:

$$M^{SCT}_{LVLH\to BODY} = \left[\begin{array}{c|ccc} B & & \overline{L \quad V \quad L \quad H} & \\ O & O_{BT}X_{BT}.x & O_{BT}X_{BT}.y & O_{BT}X_{BT}.z \\ D & O_{BT}Y_{BT}.x & O_{BT}Y_{BT}.y & O_{BT}Y_{BT}.z \\ Y & O_{BT}Z_{BT}.x & O_{BT}Z_{BT}.y & O_{BT}Z_{BT}.z \end{array}\right], \quad (11)$$

where $O_{BR}X_{BR}.x$, $O_{BR}X_{BR}.y$, $O_{BR}X_{BR}.z$ are the components of the unit vector $O_{BR}X_{BR}$; $O_{BR}Y_{BR}.x$, $O_{BR}Y_{BR}.y$, $O_{BR}Y_{BR}.z$ are the components of the unit vector $O_{BR}Y_{BR}$; $O_{BR}Z_{BR}.x$, $O_{BR}Z_{BR}.y$, $O_{BR}Z_{BR}.z$ are the components of the unit vector $O_{BR}Z_{BR}$; $O_{BT}X_{BT}.x$, $O_{BT}X_{BT}.y$, $O_{BT}X_{BT}.z$ are the components of the unit vector $O_{BT}X_{BT}$; $O_{BT}Y_{BT}.x$, $O_{BT}Y_{BT}.y$, $O_{BT}Y_{BT}.z$ are the components of the unit vector $O_{BT}Y_{BT}$; $O_{BT}Z_{BT}.x$, $O_{BT}Z_{BT}.y$, $O_{BT}Z_{BT}.z$ are the components of the unit vector $O_{BT}Z_{BT}$.

VIII) Transiting matrices from SCR and SCT body frames to corresponding reference frames, which are connected with rectenna and antenna, respectively, ARF. To determine the position of the antenna and rectenna, it will be appropriate to use rotation by two angles (mounting pitch θ_m and mounting yaw ψ_m) and set the OX-axis as the vision axis. So, when mounting pitch and roll values are equal to zero, the vision axes of the SCR and SCT are $O_{BR}X_{BR}$ and $O_{BT}X_{BT}$, respectively. Considering this, we can determine the next order of rotations:

1-st: rotation around the OZ axis ($O_{BR}Z_{BR}$ or $O_{BT}Z_{BT}$) by the angle of the mounting yaw ψ_m counterclockwise;

2-nd: rotation around the rotated axis OY ($O_{BR}Y_{BR}$ or $O_{BT}Y_{BT}$) by the angle of the mounting pitch θ_m counterclockwise.

So, the rotation matrix for SCR and SCT body frames to corresponding aperture reference frames can be written as:

$$M_{BF\to ARF}^{SCT/SCR}=\left[\begin{array}{c|ccc} & B & O & D & Y \\ \hline A & & & & \\ R & \cos\psi_m\cos\theta_m & \sin\psi_m\cos\theta_m & -\sin\theta_m & \\ F & -\sin\psi_m & \cos\psi_m & 0 & \\ & \cos\psi_m\sin\theta_m & \sin\psi_m\sin\theta_m & \cos\theta_m & \end{array}\right]. \quad (12)$$

In turn, mounting yaw ψ_m and mounting pitch θ_m are selected for SCR and SCT separately.

IX) Calculation of the targeting quaternions. Thus, having determined the transiting matrices between these reference frames (6), (7), (12)—(14), one can find the corresponding quaternions. So, the quaternion of transition from BODY to ARF can be written as follows:

$$Q_{BF\to ARF}^{SCT/SCR}=\begin{bmatrix}Q_0\\Q_x\\Q_y\\Q_z\end{bmatrix}=\begin{bmatrix}\cos\frac{\Psi_m}{2}\cos\frac{\theta_m}{2}\\-\sin\frac{\Psi_m}{2}\sin\frac{\theta_m}{2}\\\cos\frac{\Psi_m}{2}\sin\frac{\theta_m}{2}\\\sin\frac{\Psi_m}{2}\cos\frac{\theta_m}{2}\end{bmatrix}, \quad (13)$$

where Q_0 is the scalar part of the quaternion $Q_{BF\to ARF}^{SCT/SCR}$; Q_x, Q_y, Q_z are the components of the vector part of the quaternion $Q_{BF\to ARF}^{SCT/SCR}$.

The transition quaternion from LVLH to SC and SR body frames is determined using the algorithm of quaternions calculation from matrix elements [11]. So, this quaternion can be calculated from LVLH matrix elements using the next formula:

$$L_{LVLH\to BF}^{SCR/SCT}=\begin{bmatrix}L_0\\L_x\\L_y\\L_z\end{bmatrix}=\begin{bmatrix}\frac{1+M_{11}+M_{22}+M_{33}}{2\cdot\sqrt{1+M_{11}+M_{22}+M_{33}}}\\\frac{M_{23}-M_{32}}{2\cdot\sqrt{1+M_{11}+M_{22}+M_{33}}}\\\frac{M_{31}-M_{13}}{2\cdot\sqrt{1+M_{11}+M_{22}+M_{33}}}\\\frac{M_{12}-M_{21}}{2\cdot\sqrt{1+M_{11}+M_{22}+M_{33}}}\end{bmatrix}, \quad (14)$$

where $L_{LVLH\to BF}^{SCR/SCT}$ is the quaternion of transition from LVLH reference frame to corresponding SCR or SCT body reference frames; L_0 is the scalar part of the quaternion $L_{LVLH\to BF}^{SCR/SCT}$; L_x, L_y, L_z are the components of the vector part of the quaternion $L_{LVLH\to BF}^{SCR/SCT}$; M_{11}, M_{12}, M_{13}, M_{21}, M_{22}, M_{23}, M_{31}, M_{32}, M_{33} are the components of the matrix (10) or matrix (11) for SCR or SCT, respectively.

In turn, the transition quaternion from LVLH to aperture reference frames for SCR or SCT can be determined as:

$$L_{LVLH\to ARF}^{SCR/SCT}=L_{LVLH\to BF}^{SCR/SCT}\circ Q_{BF\to ARF}^{SCT/SCR}, \quad (15)$$

where $L_{LVLH\to ARF}^{SCR/SCT}$ is the transition quaternion from LVLH to SCT or SCR aperture reference frame.

Simulation results. Taking into account the technical requirements for the SEPSOG satellites of the distributed electrical-power system of the space industrial platform, the following approximate values of the mass and size parameters of the general design of the SKT and SKR have been established:

1) mass of the SCT: 1000 kg,
2) mass of the SCR: 1500 kg,
3) average value of SCT cross-section area 10 m^2,
4) average value of SCT cross-section area 15 m^2,
5) aperture mounting yaw and pitch of SCT: $\psi_m = 30$ deg, $\theta_m = 25$ deg,
6) aperture mounting yaw and pitch of SCR: $\psi_m = 30$ deg, $\theta_m = 40$ deg,
7) radius of SCT antenna aperture: 2 m,
8) radius of SCR rectenna aperture: 3 m,
9) microwave wavelength $\lambda = 1000$ GHz,
10) transmitting power (total radiated power from transmitter per second) $P_t = 10$ kW,
11) $D_{\max} = 100$ km,
12) the power density at the center of the SCR rectenna p_d on the maximal distance of microwave power transmitting $D_{\max}$ is 139.82 W/m^2.

To determine the optimal orbit parameters for SCT and SCR dislocations, it is proposed to use an application (Figure 2) that includes developed mathematical models for estimating communication session duration and the dynamic changes of targeting quaternions inflight. Considering these SCT and SCR parameters, it is proposed to analyze the efficiency of contactless microwave power transition using scenarios with the following conditions:

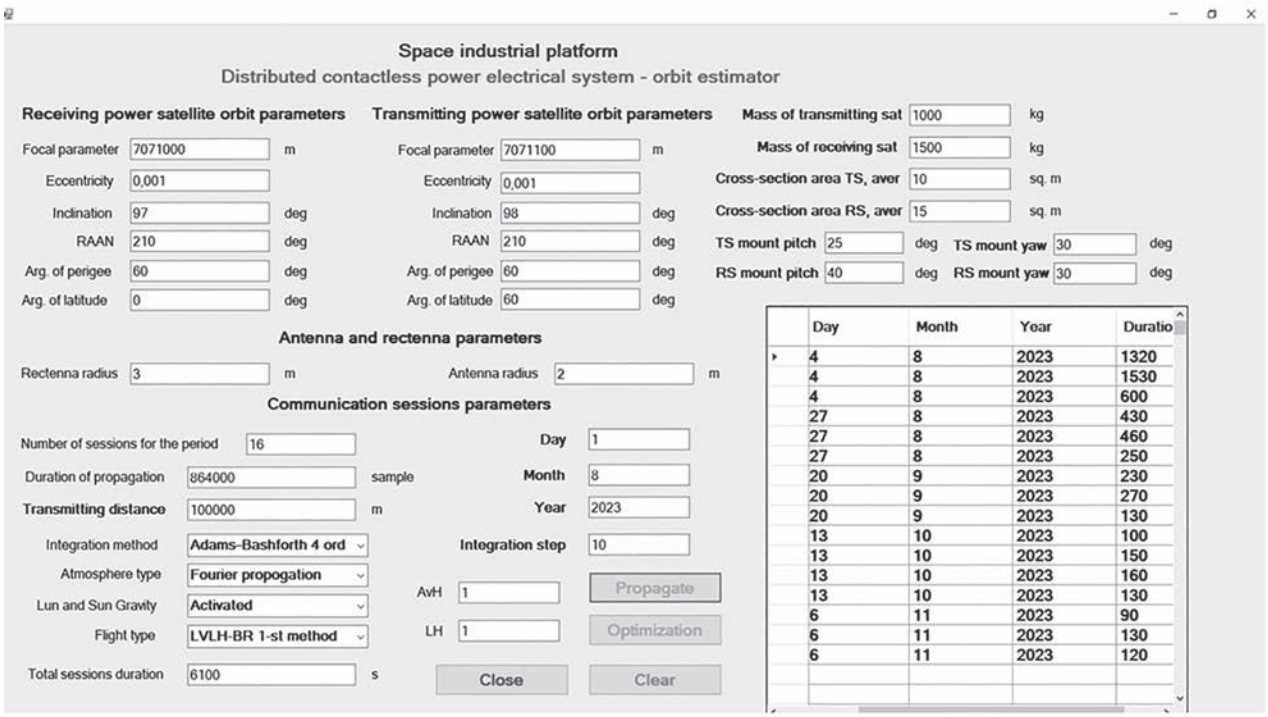

Figure 3. Simulation results of connection session estimation for Scenario A

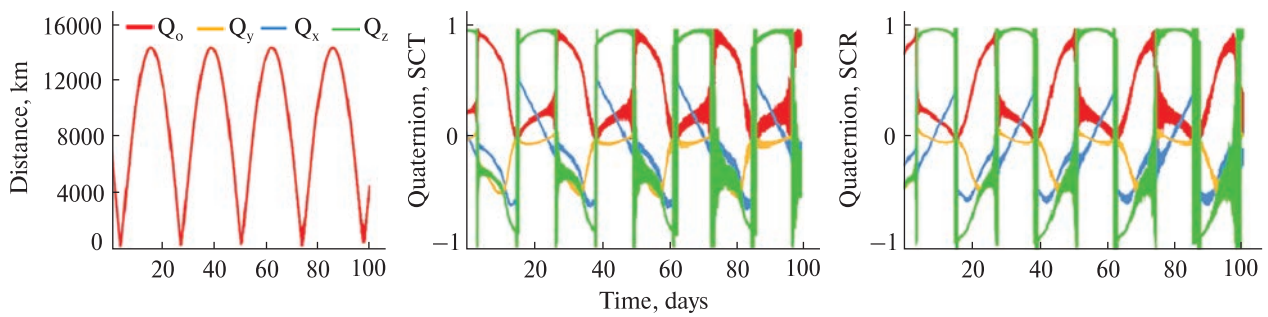

Figure 4. Relative distance between the change of SCR and SCT and the dynamics of change of SCR and SCT targeting quaternions for Scenario A

A) SCR and SCT are located in near coplanar orbits with the next initial differences: 1 deg difference in inclination, 100 m difference in altitude, and 60 deg difference in the argument of latitude.

B) SCR and SCT have coplanar orbits with an initial 100 m difference in altitude and 60 deg difference in the argument of latitude.

C) Optimization of orbital parameters by variation of the argument of perigee value and argument of latitude value.

Taking into account the expected range of space industrial platform average orbit altitudes between 600 km and 800 km, it is proposed to set the next SCT and SCR orbits for scenario A:

SCT orbit: the focal parameter is 7071100 m, eccentricity is 0.001, the inclination is 98 degrees, RAAN is 210 degrees, the argument of perigee is 60 degrees, the argument of latitude is 60 degrees.

SCR orbit: the focal parameter is 7071000 m, eccentricity is 0.001, the inclination is 97 degrees,

RAAN is 210 degrees, the argument of perigee is 60 degrees, the argument of latitude is 0 degrees.

The simulation time is set equal to 100 days and the integration step of differential equations (1) to 10 seconds. The data of orbit flight start is set to be August 1, 2023.

So, the following results were obtained (Figure 3): the total number of sessions is 16; the total duration of sessions is 6100 s. Based on the obtained results (Figure 3), we can consider that there are only 5 full sessions, which are divided into 3 or 4 subperiods. This is evident from the total number of distance convergences between SCR and SCT (Figure 4).

In turn, these breaks in energy transmission sessions can be explained by the temporary exit of SCR or SCT beyond the limits of the maximum contactless transmission distance (Figure 5). This is caused to a greater extent by the impact of perturbations of the nonlinearity of the Earth's gravitational potential on SCR and SCT orbit motion and to a lesser extent by the impact of gravitational perturbations of the Sun and Moon. Also, on the targeting quaternions of SCT $L^{SCT}_{LVLH\to BF}$ and SCR $L^{SCR}_{LVLH\to BF}$ current body frame orientation relative to the LVLH frame (Figure 4), it can be seen that at the moments of transmission sessions, there is a rather strong dynamics of their changes, which is oscillatory in nature. As an example, consider changing the SCT to SCR targeting quaternion $L^{SCT}_{LVLH\to BF}$ at the time of the first session of contactless power transmitting (Figure 5).

The dependence of the $L^{SCT}_{LVLH\to BF}$ on local onboard time (time which is measured from the SCT and SCR flight simulation beginning) is presented in Figure 6. From Figure 6, it can be seen that during the first session, the dynamics of the targeting quaternion change is significant and the SCT has to perform a large number of maneuvers during target tracking, which increases the requirements for the AOCS of the SCT. Similar dynamics of targeting quaternion changes were observed during other sessions for both SCT and SCR.

In scenario B, it is proposed to model orbital motion with parameters similar to scenario A, setting the SCT and SCR orbits to the same inclination of 98 degrees. In this case, the results show a significant increase in the total duration of sessions per 100 days from 6100 s (Scenario A) to 40210 s (scenario B). In

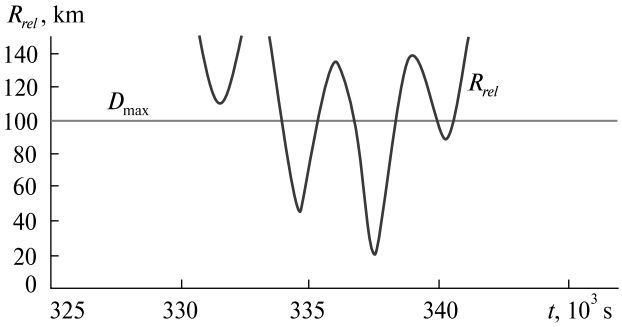

Figure 5. Breaks of contactless energy transmitting during the first communication session for Scenario A

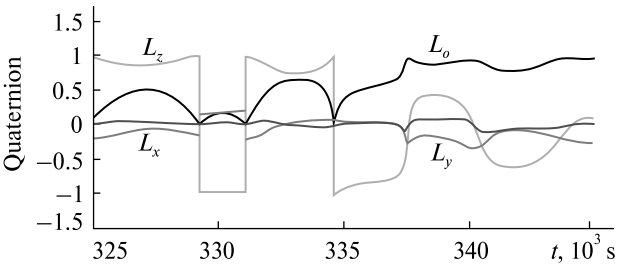

Figure 6. SCT to SCR targeting quaternion change during the first communication session for Scenario A

turn, the number of sessions significantly decreases to 7 (in comparison with 16 in scenario A), which means that the number of session breaks is reduced too (Figure 7 and Figure 8).

It can also be seen from Figure 8 that the dynamics of the changes in the targeting quaternions for SCT $L^{SCT}_{LVLH\to BF}$ are significantly lower compared to scenario A. For detailed analysis, similar to Scenario A, using output data for the first communication session, it is proposed to plot the change in the relative distance between SCT and SCR (Figure 9), as well as the targeting quaternion from SCT to SCR $L^{SCT}_{LVLH\to BF}$ (Figure 10).

Based on the obtained results in scenario B, it can be concluded that coplanar orbits are significantly better for SCR and SCT locations, which can be explained by the next peculiarities:

– using coplanar orbits allows us to increase the total time of communication sessions duration,

– no breaks in power transmission sessions (Figure 9), which can be in the cases when SCR and SCT

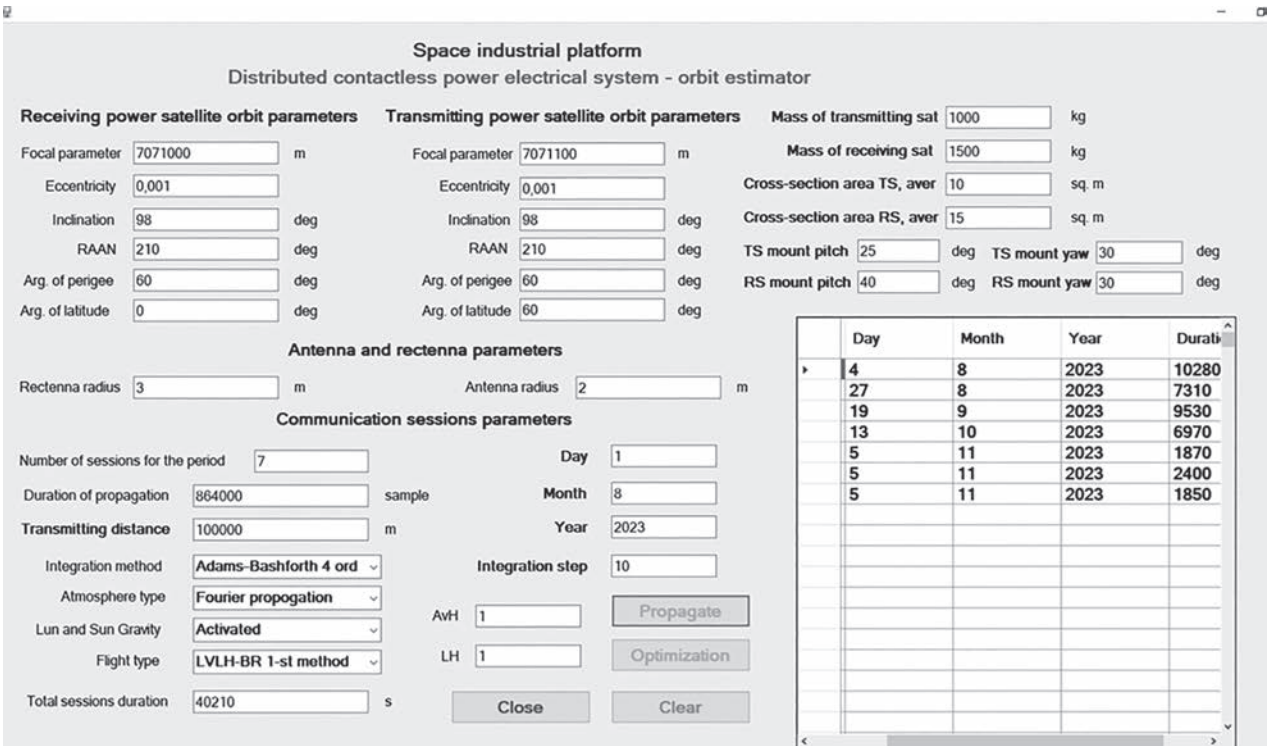

Figure 7. Simulation results of connection session estimation for Scenario B

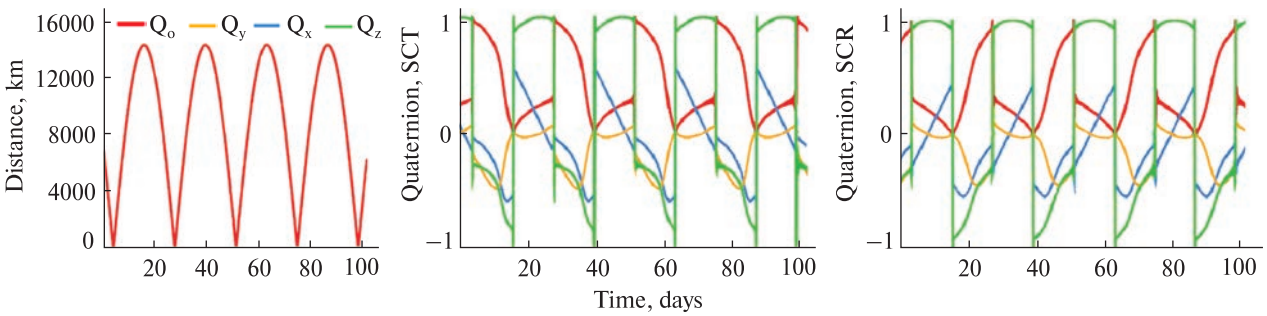

Figure 8. Relative distance between the change of SCR and SCT and the dynamics of change of SCR and SCT targeting quaternions for Scenario B

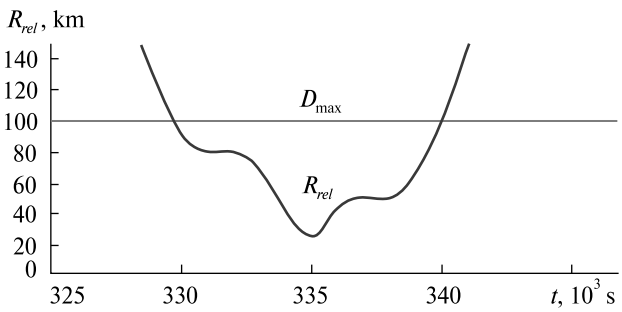

Figure 9. Change in the relative distance between SCT and SCR during the first communication session for Scenario B

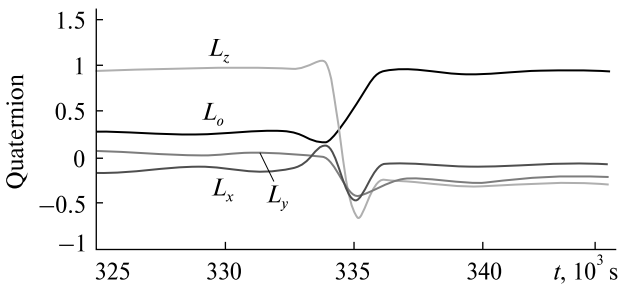

Figure 10. SCT to SCR targeting quaternion change during the first communication session for Scenario B

go beyond the maximum distance of contactless microwave power transmission (Figure 5),

– the maneuvering requirements for SCR and SCT are significantly reduced, which decreases the requirements for their AOCS systems performance (Figure 10).

In turn, these orbital parameters of SCT and SCR also cannot be considered fully optimal. Taking this into account, the tasks of optimization occur with this framework. So, it has been proposed to develop the optimization method, which is based on gradient [16] and coordinate descent methods [21], to determine the maximum value of total session duration per defined period (in this simulation, it is 100 days). It is obvious that, having determined that coplanar orbits are the most rational for the SCT and SCR locations, only orbital elements that are responsible for the shape of the orbit (focal parameter of the orbit and eccentricity), its position relative to the attracting center (the argument of perigee), and the initial position of the spacecraft in the orbit (initial SCR and SCT arguments of latitude) can be optimizing parameters. Considering this, the optimization function can be written as follows:

$$T_{c.s.} = \arg\left[\Phi\left(p,e,\omega,u\right)\right] \to \max_{\substack{p\in\mathbb{R}\\ e\in\mathbb{R}\\ \omega\in\mathbb{R}\\ u\in\mathbb{R}}}, \qquad (16)$$

where $T_{c.s.}$ is the time of the total duration of sessions, $\Phi\left(p,e,\omega,u\right)$ is the functional which describes dependence $T_{c.s.}$ on optimizing parameters.

In turn, taking into account the nonlinearity of the functional (16), which is dependent on the results of solutions of nonlinear differential equations (1), the use of all 4 optimizing parameters will make the optimization algorithm much harder. Thus, it is proposed to reduce the number of optimizing parameters in the gradient method by choosing the most significant parameters, the change of which has the greatest impact on the change in the optimized value of the functional. To do this, we first propose to analyze how the change in the shape of the orbit affects the change in $T_{c.s.}$. Considering this, the two last parameters, ω and u, are set as constants in functional (16), while p and e are proposed to vary. In this experiment, we accept the varying eccentricity and the semi-major axis of the SCT and the following other orbit parameters:

SCT orbit*:** we accept the following: focal parameter is ***variable; eccentricity is ***variable***; inclination is 98 degrees; RAAN is 210 degrees; argument of perigee is 60 degrees; argument of latitude is 60 degrees.

***SCR orbit*:** we accept the following: focal parameter is 7071000 m; eccentricity is 0.001; inclination is 98 degrees; RAAN is 210 degrees; argument of perigee is 60 degrees; argument of latitude is 0 degrees.

The results of this numerical experiment are presented in Table 1.

Based on the results of Table 1, it can be concluded that a significant increase in the eccentricity value of the SCT orbit leads to a considerable decrease in $T_{c.s.}$, which can be observed in experiment 1. In turn, no significant deviations in parameter $T_{c.s.}$ have been observed in numerical experiments from 2 to 21.

It is proposed to organize the data in Table 1 by creating an interval variation series for statistical processing. The interval variation series is presented in Table 2.

The corresponding histogram of interval variation series (Table 2) is presented in Figure 11.

Further, the interval variation series (Figure 11) was tested for the correspondence to a normal distribution using the H_0 hypothesis and Pearson's Goodness-of-Fit Test. To achieve this, the calculation of the main statistical indicators was made. These indicators are:

- Mean

$$\overline{T}_{c.s.} = \frac{\sum_{i=2}^{21} T_{c.s.i} n_i}{n},$$

where n=20, $T_{c.s.i}$ is the *i-th* numerical experiment in Table 1,

- Variance

$$DT_{c.s.} = \frac{\sum_{i=2}^{21} \left(T_{c.s.i} - \overline{T}_{c.s.}\right)^2 n_i}{n},$$

- Corrected variance

$$ST^2_{c.s.} = \frac{n}{n-1} DT_{c.s.}$$

using Bessel's correction,

- Standard deviation $\sigma T_{c.s.} = \sqrt{DT_{c.s.}}$,

Table 1. **The results of $T_{c.s.}$ change while varying the eccentricity and focal parameter of the SCT orbit**

Number of the numerical experiment	Eccentricity e and focal parameter p	Time of total duration of sessions $T_{c.s.}$, s per 100 days	Number of connection sessions per 100 days
I	**II**	**III**	**IV**
1	e=0.01 p=7071100 m	30080	18
2	e=0.005 p=7071100 m	38110	13
3	e=0.0005 p=7071100 m	41690	6
4	e=0.0001 p=7071050 m	39820	6
5	e=0.005 p=7071150 m	38610	11
6	e=0.003 p=7071080 m	42950	10
7	e=0.001 p=7071070 m	40850	7
8	e=0.002 p=7071070 m	45850	6
9	e=0.002 p=7071030 m	46850	6
10	e=0.003 p=7071030 m	43340	9
11	e=0.0015 p=7071030 m	41630	7
12	e=0.0025 p=7071060 m	43070	8
13	e=0.002 p=7071010 m	39260	6
14	e=0.0015 p=7071015 m	35520	8
15	e=0.004 p=7071040 m	37610	10
16	e=0.0001 p=7071200 m	37960	6
17	e=0.0015 p=7071035 m	36100	6
18	e=0.0015 p=7071070 m	41520	6
19	e=0.0025 p=7071080 m	43260	8
20	e=0.003 p=7071020 m	40090	9
21	e=0.002 p=7071050 m	41550	6

• Corrected standard deviation

$$ST_{c.s.} = \sqrt{ST^2_{c.s.}}\ .$$

The obtained values of these indicators are follows: $\overline{T}_{c.s.} = 40775$ s, $DT_{c.s.} = 8836875$ s^2, $ST^2_{c.s.} = 9301973.684$ s^2, $\sigma T_{c.s.} = 2972.688177$ s, $ST_{c.s.} = 3049.913718$ s. Using algorithm [6], the obtained chi-squared test statistic $\chi^2_{n_2}$ is equal to 5.704462. In turn, the critical value of $\chi^2_{cr}(\alpha_1)$ for the interval variation series (Table 2) with a level critical value $\alpha_1 = 0.05$ is equal to 11.1. Thus, $\chi^2_n < \chi^2_{cr}(\alpha_1)$ and H_0 hypothesis can be accepted.

Then, for comprehensive estimation, confidence intervals for mean, corrected variance, and corrected standard deviation were calculated, assuming a normal distribution of the general population. Using standards [13], it can be written as follows:

$$\overline{T}_{c.s.} - ST_{c.s.}\frac{t_{1-\alpha/2}(\nu)}{\sqrt{n}} < \overline{T}_{c.s.} < \overline{T}_{c.s.} + ST_{c.s.}\frac{t_{1-\alpha/2}(\nu)}{\sqrt{n}}, \quad (17)$$

$$\frac{\sum_{k=2}^{21}\left(T_{c.s.k} - \overline{T}_{c.s.}\right)^2}{\chi^2_{1-\alpha/2}(\nu)} < ST^2_{c.s.} < \frac{\sum_{k=2}^{21}\left(T_{c.s.k} - \overline{T}_{c.s.}\right)^2}{\chi^2_{\alpha/2}(\nu)}, \quad (18)$$

$$\sqrt{\frac{\sum_{i=2}^{21}\left(T_{c.s.i} - \overline{T}_{c.s.}\right)^2}{\chi^2_{1-\alpha/2}(\nu)}} < ST_{c.s.} < \sqrt{\frac{\sum_{i=2}^{21}\left(T_{c.s.i} - \overline{T}_{c.s.}\right)^2}{\chi^2_{\alpha/2}(\nu)}}, \quad (19)$$

where $T_{c.s.k}$ are the $T_{c.s.}$ from Table 1, $\nu = n-1$ is the degrees of freedom, $t_{1-\alpha/2}(\nu)$ is the Student's t-distribution quantile function with the probability $(1-\alpha/2)$, $\chi^2_{1-\alpha/2}(\nu)$ is the χ^2 distribution quantile function with the probability $(1-\alpha/2)$; $\chi^2_{\alpha/2}(\nu)$ is the χ^2 distribution quantile function with the probability $\alpha/2$.

We assumed α equal to 0.01. So, the calculated values of the confidence intervals are as follows:

a) $38812.25738 < \overline{T}_{c.s.} < 42737.74262$,

b) $4432605.43 < ST^2_{c.s.} < 24988403.5$,

c) $2105.375 < ST_{c.s.} < 4998.84$.

The statistical processing shows that with the probability of 99 % the values of mean, variance, and standard deviation will be within these confidence intervals. Considering previously calculated values of mean, variance, and standard deviation, it can be concluded that there are no significant deviations of $T_{c.s.}$ with small variations in the eccentricity and focal parameter. Thus, these parameters can be excluded from functional (16) and rewritten as

$$T_{c.s.} = \arg\left[\Phi\left(\omega, u\right)\right] \to \max_{\substack{\omega\in\mathbb{R} \\ u\in\mathbb{R}}}.$$

Using the rule of functional differentiation, the partial derivatives of $T_{c.s.}$ with respect to the argument of perigee ω and argument of latitude u can be defined as:

1) $\dfrac{\partial T_{c.s.}}{\partial \omega} = \dfrac{\partial \Phi\left(\omega, u\right)}{\partial \omega}$,

2) $\dfrac{\partial T_{c.s.}}{\partial u} = \dfrac{\partial \Phi\left(\omega, u\right)}{\partial u}$.

In turn, using numerical differentiation, these partial derivatives can be written in the following form:

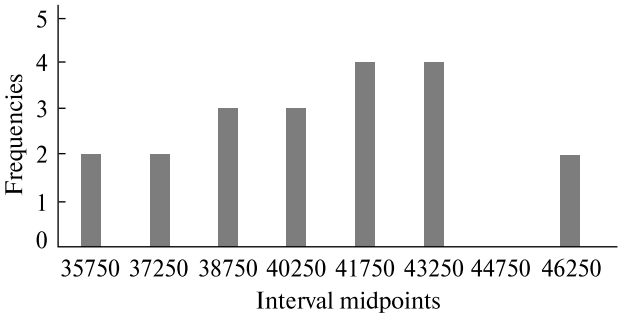

Figure 11. The interval variation series of $T_{c.s.}$

Table 2. **The interval variation series of $T_{c.s.}$ distribution**

Intervals	Intervals midpoints $T_{c.s.i}$	Frequencies n_i
35000—36500	35750	2
36500—38000	37250	2
38000—39500	38750	3
39500—41000	40250	3
41000—42500	41750	4
42500—44000	43250	4
44000—45500	44750	0
45500—47000	46250	2

$$\frac{\partial\Phi(\omega,u)}{\partial\omega}=\frac{\Phi(\omega+h,u)-\Phi(\omega-h,u)}{2h},$$
$$\frac{\partial\Phi(\omega,u)}{\partial u}=\frac{\Phi(\omega,u+h)-\Phi(\omega,u-h)}{2h}, \quad (20)$$

where h is the step of differentiation.

So, the module of gradient value can be defined as follows:

$$\left|\nabla T_{c.s.}\right|=\sqrt{\left(\left.\frac{\partial\Phi(\omega,u)}{\partial\omega}\right|_{\substack{u_k\\ \omega_k}}\right)^2+\left(\left.\frac{\partial\Phi(\omega,u)}{\partial u}\right|_{\substack{u_k\\ \omega_k}}\right)^2}, \quad (21)$$

where ω_k is the argument of perigee value on the *k-th* iteration of optimization, u_k is the argument of latitude value on the *k-th* iteration of optimization.

However, given the significant nonlinearity of this functional, which depends on the solution of the nonlinear problem of predicting the spacecraft's motion, the standard stopping criteria when searching for the minimum and maximum using the gradient method are problematic for application. It can be explained by the following factors:

1) A large number of local minima and maxima, which makes it impossible to use the stopping criterion based on the zero gradient and step minimization.

2) A large number of high peaks and smoothness problems, which entails gradient module jumps.

In turn, the method of coordinate descent, in this case, requires significant computational costs and time. Considering this, it is proposed to decompose the optimization process

$$T_{c.s.}=\arg\left[\Phi(\omega,u)\right]\to\max_{\substack{\omega\in\mathbb{R}\\ u\in\mathbb{R}}}$$

using the combined approach of coordinate descent and gradient methods. This can be implemented using the following algorithm:

Step 1. Set ω to a constant and vary u from minimum to maximum with a constant step (given that u has angular value in the range from 0 deg to 360 deg, these values can be the minimum and maximum values in the optimization range). At each step, the current value of $T_{c.s.}$ and gradient module (21) are calculated.

Step 2. Analysis of the dynamics of the change of obtained $T_{c.s.}$ values and the change of gradient values. Searching the maximum value of $T_{c.s.}$.

Step 3. Set u to a constant and vary ω from minimum to maximum with a constant step (given that ω has angular value in the range from 0 deg to 360 deg, these values can be the minimum and maximum values in the optimization range). At each step, the current value of $T_{c.s.}$ and gradient module (21) are calculated.

Step 4. Analysis of the dynamics of obtained $T_{c.s.}$ values' change and gradient values' change. Searching the maximum value of $T_{c.s.}$.

Step 5. Comparison of the obtained dynamics of the change in the gradient and $T_{c.s.}$ time for two independent variations of the parameters u and ω. Choosing the most significant parameter that affects maximization $T_{c.s.}$.

Using this algorithm, it is proposed to carry out the numerical experiment and SCT, SCR flight simulation to determine the maximum value of $T_{c.s.}$.

SCT and SCR orbit parameters for ***step 1***:

SCT orbit. The focal parameter is 7071100 m; eccentricity is 0.001; inclination is 98 degrees; RAAN is 210 degrees; argument of perigee is 60 degrees; argument of latitude is variated in the range from 9 deg to 361 deg with the step 8 deg.

SCR orbit. The focal parameter is 7071000 m; eccentricity is 0.001; inclination is 98 degrees; RAAN is 210 degrees; argument of perigee is 60 degrees; argument of latitude is 0 degrees.

Step of differentiation (20) $h=1$ deg.

So, after step 1, it has been obtained the following results.

The maximum value of $T_{c.s.}$ is 1185420 s, where SCT $u=361$ deg (Figure 12, *a*). According to small gradient changes $\left|\nabla T_{c.s.}\right|\to\min$ at the $u=361$ deg (Figure 12, *b*), this point lies near maximum $T_{c.s.}$. In turn, a significant increase in $T_{c.s.}$ is observed in the range from 0 deg to 20 deg difference in the argument of latitude between SCT and SCR. Also, there are 2 "dead zones" where it hasn't been observed any communications ($T_{c.s.}=0$) in the SCT u range from 166 deg to 196 deg and from 337 deg to 359 deg during these 100 days (calculated from August 1, 2023, 00:00:00). These values are absolute minimums because the $\left|\nabla T_{c.s.}\right|=0$ too.

For step 3, it is proposed to analyze the ω change influence on $T_{c.s.}$ change. By setting the constant $u=17$ deg (corresponding to the range with a sig-

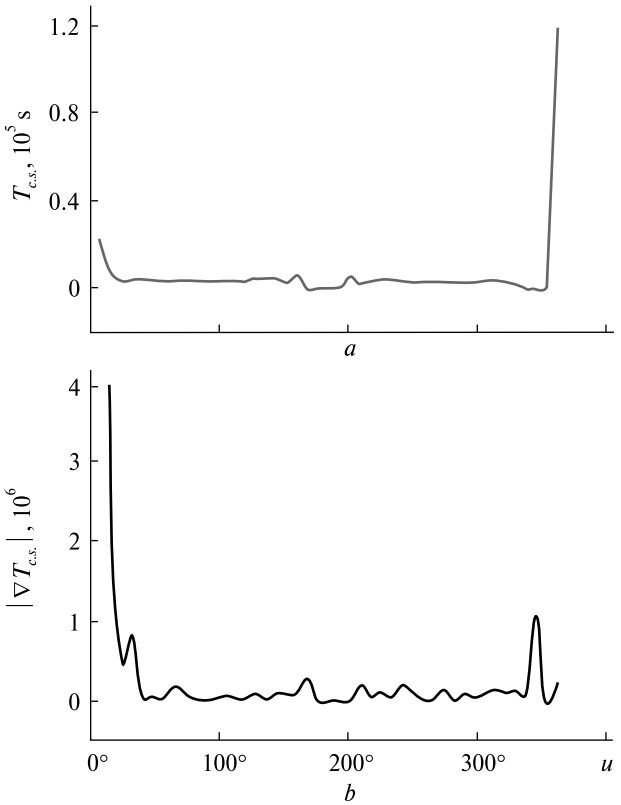

Figure 12. The dependence of $T_{c.s.}$ (*a*) and $|\nabla T_{c.s.}|$ (*b*) change while variating *u*

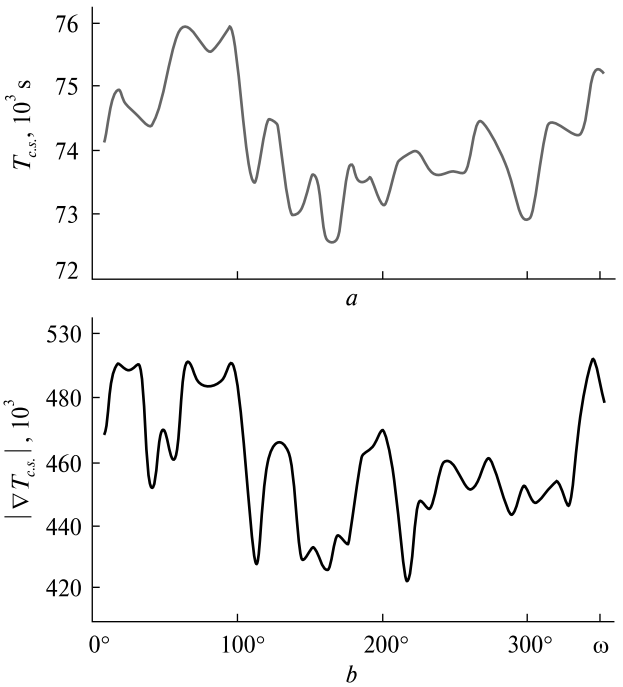

Figure 13. The dependence of $T_{c.s.}$ (*a*) and $|\nabla T_{c.s.}|$ (*b*) change while variating ω

nificant increasing in $T_{c.s.}$) for the determined SCT orbit at step 1 and varying ω in the range from 8 deg to 352 deg with a step of 8 deg and $h = 1$ deg, the following results were obtained (Figure 13, *a*).

According to the obtained results (Figure 13, *b*), it is clear that the change in ω doesn't have a significant effect on the change in $T_{c.s.}$. The range of Ts lies within the range of this value with small variations of the eccentricity and focal parameter (Table 1). Also, taking into account many small fluctuations in the gradient module $|\nabla T_{c.s.}|$, it can be concluded that varying the parameter ω leads to a large number of local maxima and minima of $T_{c.s.}$, which lie in the range from 72500 s to 76000 s. Based on this, the effect of changing the ω parameter on time $T_{c.s.}$ can also be considered insignificant.

Thus, only the orbit argument of latitude u remains a significant parameter of influence on the $T_{c.s.}$ value, which is the key when optimizing the SCT orbit to obtain the maximum duration with contactless energy transfer over a certain period. In this case, the optimal time (maximum) is obtained for the difference of the argument of latitude between SCT and SCR of 1 degree (1185420 s, where SCT $u = 361$ deg). However, under these conditions, only one connection session has been observed for 100 days. The simulation period has been extended to 3000 days to estimate the frequency of contactless energy transfer sessions. The results showed that the frequency of communication sessions for contactless power transiting from SCT to SCR decreases significantly (approximately 1 session per 2500 days in Figure 14), which cannot be optimal on this side.

Thus, taking into account these peculiarities of the translational relative and attitude motion of SCT and SCR, it can be developed the following methodology for selecting their dislocation orbits. This methodology can be presented as a sequence of following procedures:

I) Taking into account the technical parameters of SCT and SCR, the determination of the maximum

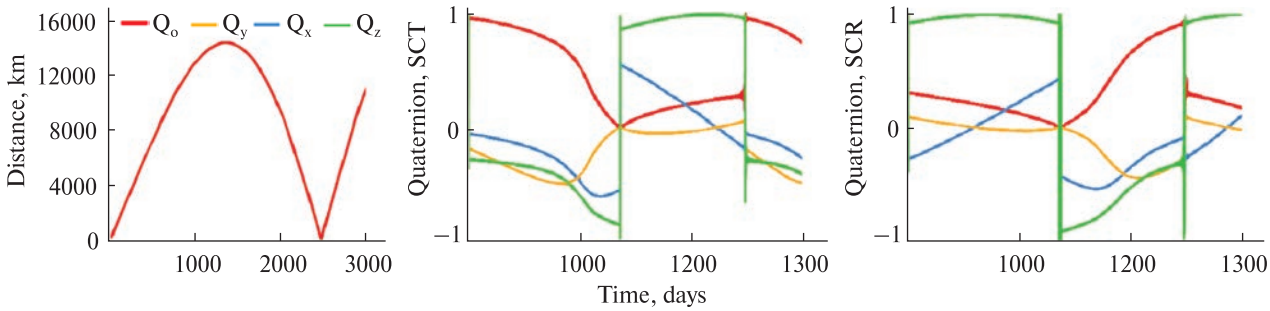

Figure 14. Relative distance between the change of SCR and SCT and the dynamics of change of SCR and SCT targeting quaternions over the maximum time $T_{c.s.}$

distance of contactless power transition between SCT and SCR $D_{\max}$.

II) Determination of the SCR orbit, taking into account the orbit of the space industrial platform.

III) Determination of the power budget requirements for the space industrial platform.

IV) Using the calculus of variations and an optimization algorithm, select an orbit for SCT, taking into account the following:

a) peculiarities of SCT and SCR AOCS and maneuvering properties,

b) time of total duration of sessions $T_{c.s.}$,

c) periodicity of connection sessions according to space industrial platform power budget requirements,

d) estimated targeting quaternion changes $L^{SCR/SCT}_{LVLH\to BF}$ during connection sessions, taking into account SCT and SCR maneuvering restrictions,

e) searching the optimal value of $T_{c.s.}$, taking into account requirements of connection sessions periodicity and SCT, SCR contactless power storage and transiting system peculiarities.

Discussion. Contactless power transition throughout the space between two satellites was proposed in research works [1, 5]. In turn, these works consider the possibility of contactless power transmission at close distances (hundreds of meters between SCR and SCT). Given the significant electrical power required for the SIP, as well as the significant presence of auxiliary service spacecraft, close-range contactless power transmission is difficult and can cause considerable electrical interference to other SIP devices. Considering this, it was proposed to separate the SIP receiver from the platform itself [20]. Based on this, a problem arose regarding the rational choice of SCT and SCR orbits that satisfy the requirements for SIP powering. One of the key indicators on which the orbit selection algorithm is based is the maximum range of contactless power transmission from SCT to SCR (3)—(5). Taking into account the nonlinearity of the space flight dynamics under the influence of environmental perturbations, the authors proposed to estimate the current relative distance between the power satellites when predicting the orbital motion of the SCR and SCT separately. Considering the peculiarities of the relative motion of spacecraft on perturbed orbits it was revealed that these spacecrafts have periodicity of approaches and distances. Based on it, the condition (3) of contactless power transmitting between SCT and SCR has been formulated. Using this condition (3), an algorithm for measuring the duration of communication sessions (power transmitting session) has also been formulated.

The second key parameter in contactless power transfer from SCT to SCR is the change in relative angular position during a power transfer session. Considering the presence of the need for large turns of the SCT and SCR when pointing the receiver and transmitter apertures, the use of the quaternion calculus instead of the angles has been proposed. This avoided singularities for large-angle rotations. In turn, assessments of the dynamics of the orientation quaternion change of SCT and SCR are key in forming requirements for their AOCS systems which will be needed in further research.

Methodical approaches to the selection of their optimal parameters have been proposed in the study of SCT and SCR orbits. Given the nonlinearity of

the functional (16), it has been proposed to conduct a comprehensive study to identify the most significant parameters influencing the change in the time of total duration of communication sessions. On this basis, we decomposed the problem of optimal parameters search into three stages:

1) Statistical processing of the small focal parameter and eccentricity variations influencing the change in the time of total duration of communication sessions (17)—(19).

2) Development and use of the combined method based on the coordinate descent optimization and gradient optimization to analyze the influence of the argument of latitude variations and argument of perigee variations.

3) Analysis of periodicity of power transmitting sessions.

Using this method, it has been found that the orbit argument of latitude u is the most significant parameter, which affects the time of total communication sessions' duration change. The advantage of this method is the speed of searching for optimal parameters due to the exclusion of insignificant optimized values. The disadvantage of this method is the limitation of the accuracy of the search for optimal parameters due to the exclusion of insignificant optimized values.

Conclusions. 1. The mathematical model of SEPSOG orbital translational and relative motion has been determined. It has been proposed to use the orbit motion propagator, taking into account the impact of environmental perturbations. Based on this model, the corresponding software has been developed. Using this software allows us to analyze the relative motion of the spacecraft transmitter and spacecraft receiver, which also allows the calculation of contactless power transmitting sessions per any period.

2. The mathematical model of targeting quaternions has been developed for spacecraft transmitter and receiver pointing during a power transmitting session. This allowed us to estimate the dynamics of targeting quaternion changes during power transmitting sessions and develop the requirements for spacecraft transmitter and spacecraft receiver AOCS systems' performance.

3. The numerical experiment of spacecraft receiver and transmitter orbital translational and relative motion has been carried out. It has been determined that coplanar orbits are the most optimal for SEPSOG module dislocation. It can be explained by the minimal maneuvering requirements for both the receiver and transmitter of the spacecraft during a power transmitting session, as well as a significant increase in the total duration of sessions (by several orders of magnitude) in these orbits.

4. The methodology for determining the most optimal orbital parameters for the SEPSOG spacecraft's location has been developed. This algorithm includes statistical processing, gradient optimization elements, and coordinate descent optimization elements. Using this combination has allowed us to determine the most significant parameter, influencing the change of total duration of communication sessions. Considering this, the methodology of the rational orbital parameters has been developed. Implementation of this methodology can allow us to select the rational orbits for the SEPSOG spacecraft depending on the receiver orbit.

Acknowledgements. *The authors declare the following financial interests/personal relationships that may be construed as potentially competing interests: H. Lu reports that the financial support was provided by the China Postdoctoral Science Foundation (No. 2023M732862) and the Natural Science Foundation of Chongqing, China (No. 2023NSCQMSX2403). C. Wang reports that the financial support was provided by the Key Research and Development Program of Shaanxi(2023-GHZD-32), the Fundamental Research Funds for the Central Universities, and the National Natural Science Foundation of China (Grant No. 62273277). E. Lapkhanov reports that financial support was provided under grants of the National Academy of Sciences of Ukraine to research laboratories/groups of young scientists of the National Academy of Sciences of Ukraine for research in the priority areas of science and technology development (Grant No. 0122U002079).*

REFERENCES

1. Aditya B., Hongru C., Yasuhiro Y., Shuji N., Toshiya H. (2021). Verify the Wireless Power Transmission in Space using Satellite to Satellite System. *Int. J. Emerging Technologies*, **12**(2), 110—118.
2. Alpatov A. P., Khoroshylov S. V., Maslova A. I. (2019). *Contactless de-orbiting of space debris by the ion beam. Dynamics and control*. Kyiv: Akademperiodyka, 170 p.
3. Alpatov A., Kravets V., Kravets V., Lapkhanov E. (2021). Representation of the kinematics of the natural trihedral of a spiral-helix trajectory by quaternion matrices. *Trans. Machine Learning and Artificial Intelligence*, **9**(4), 18—29. https://doi.org/10.14738/tmlai.94.10523
4. Bergsrud C., Bernaciak R., Kading B., McClure J., Straub J., Shahukhal S., Williams K. (2021). SunSat Design Competition 2013—2014 Third Place Winner – Team University of North Dakota: Nano SSP Satellite. *Online J. Space Communication*, **11**(18). URL: https://ohioopen.library.ohio.edu/cgi/viewcontent.cgi?article= 1444&context=spacejournal (Last accessed: 16.08.2023).
5. Bergsrud C., Straub J. (2014). A space-to-space microwave wireless power transmission experiential mission using small satellites. *Acta Astronautica*, **103**, 193—203. https://doi.org/10.1016/j.actaastro.2014.06.033
6. Chang S., Li D., Qi Y. (2023). Pearson's goodness-of-fit tests for sparse distributions. *J. Appl. Statistics*, **50**(5), 1078—1093. doi: 10.1080/02664763.2021.2017413
7. Chaudhary K., Kumar D. (2018). Satellite solar wireless power transfer for baseload ground supply: clean energy for the future. *Eur J. Futures Res.*, **6**(9). https://doi.org/10.1186/s40309-018-0139-7
8. Curtis H. (2019). *Orbital Mechanics for Engineering Students* (4th ed.). Butterworth-Heinemann, 692 p.
9. Fortescue P., Stark J., Swinerd G. (2011). *Spacecraft systems engineering*. John Wiley & Sons Ltd. Chichester, 724 p.
10. Golubek A. V., Filipenko I. M., Tatarevskii K. E. (2020). *A Priory Estimation of Orbital Injection Accuracy for Modern Launch Vehicles with a Strapdown Inertia Navigation System*. Dnipro: LIRA, 187 p. [in Russian].
11. Gordeev V. N. (2016). *Quaternions and biquaternions with applications in geometry and mechanics*. Kyiv: Publishing house "Steel", 316 p.
12. Gosavi S. S., Mane H. G., Pendhari A. S., Magdum A. P., Deshpande S., Baraskar A., Jadhav M., Husainy A. (2021). A review on space based solar power. *J. Thermal Energy Systems*, **6**(1), 16—24. doi:10.46610/jotes.2021.v06i01.003
13. ISO 16269-6:2014. Statistical interpretation of data. Part 6: Determination of statistical tolerance intervals. URL: https://www.iso.org/obp/ui/en/#iso:std:iso:16269:-6:ed-2:v1:en (Last accessed: 16.08.2023).
14. Khoroshylov S. V. (2009). On algorithmic support of orientation control of solar space power plants. Part 1. *System technologies*, **61**(2), 153—167 [in Russian].
15. Landis G. A. (2006). *Re-evaluating satellite solar power systems for Earth*. IEEE 4th World Conf. on Photovoltaic Energy Conversion (Waikoloa, HI, USA, 7—12 May). doi: 10.1109/WCPEC.2006.279877
16. Lockett A. J. (2020). Review of Optimization Methods. General-Purpose Optimization Through Information Maximization. Natural Computing Series. Springer, Berlin, Heidelberg. https://doi.org/10.1007/978-3-662-62007-6_2
17. Makarov A. L., Khoroshilov S. V. (2012). Attitude control of solar battery and transmitting antenna for space solar power satellite. *Kosm. nauka tehnol.,* **18**(3), 3—9. doi: 10.15407/knit2012.03.003
18. Mankins J. C. (2014). *The Case for Space Solar Power*. Virginia Edition Publishing, LLC, 580 p.
19. National Geospatial-Intelligence Agency (NGA) standardization document (2008). Department of Defense, World Geodetic System 1984, 208 p. URL: https://nsgreg.nga.mil/doc/view?i=4085 (Last accessed: 16.08.2023).
20. Palii O. S., Lapkhanov E. O., Svorobin D. S. (2022). Model of distributed space power system motion control. *Technical mechanics*, **4**, 35—50. doi: 10.15407/itm2022.04.035
21. Rabanser S., Neumann L., Haltmeier M. (2019). Analysis of the Block Coordinate Descent Method for Linear Ill-Posed Problems. *SIAM J. Imaging Sci.*, **12**(4), 1808—1832. doi:10.1137/19m1243956
22. Reshetnev M. F., Lebedev V. A., Bartenev V. A., Krasil'shchikov M. N., Malyshev V. A. (1988). *Control and navigation of artificial Earth satellites in near-circular orbits*. Mashinostroenie Publishing House, 336 p. [in Russian]
23. Sasaki S. and JAXA Advanced Mission Research Group (2009). SSPS development road map. IAC-09.C3.1.4. URL: http://www13.plala.or.jp/spacedream/PDFSPSENG12.pdf (Last accessed: 16.08.2023).
24. Wang E., Wu S., Liu Y., Wu Z., Liu X. (2019). Distributed vibration control of a large solar power satellite. *Astrodynamics*, **3**(2), 189—203. https://doi.org/10.1007/s42064-018-0046-5
25. Yermoldina G. T., Suimenbayev B. T., Sysoev V. K., Suimenbayeva Zh. B. (2018). Features of Space Solar Power Station Control System. *Acta Astronautica*, **158**, 111—120. https://doi.org/10.1016/j.actaastro.2018.04.001
26. Zbrutskii A. V., Ganzha A. P. (2011). *Navigation of the Earth remote sensing satellite by land surface imagery*. Kyiv: National Technical University "Kyiv Polytechnic Institute" Publishing House, 160 p. [in Russian]

Стаття надійшла до редакції 04.02.2024 *Received 04.02.2024*
Після доопрацювання 04.02.2024 *Revised 04.02.2024*
Прийнято до друку 02.05.2024 *Accepted 02.05.2024*

А. П. Алпатов[1,2], зав. відділу системного аналізу та проблем керування, проф.,
д-р техн. наук, член-кор. НАН України
ORCID: https://orcid.org/0000-0003-4411-2250
E-mail: aalpatov@ukr.net
***Ч. Ван*[2],** д-р філософії, проф.
ORCID: https://orcid.org/0000-0002-1358-7731
E-mail: wangcq@nwpu.edu.cn
Х. Лу[2,3], д-р філософії, докторант
ORCID: https://orcid.org/0000-0003-4695-3424
E-mail: luhs@nwpu.edu.cn
Е. О. Лапханов[1], д-р філософії, наук. співроб.
ORCID: https://orcid.org/0000-0003-3821-9254
E-mail: ericksaavedralim@gmail.com

[1] Інститут технічної механіки Національної академії наук України
і Державного космічного агентства України
вул. Лешко-Попеля 15, Дніпро, Україна, 49005
[2] Школа автоматизації, Північно-Західний політехнічний університет
Сіань, Китай
[3] Інноваційний центр Чунціна, Північно-Західний політехнічний університет
Чунцін, Китай

ВИБІР ОРБІТИ КОСМІЧНОЇ ІНДУСТРІАЛЬНОЇ ПЛАТФОРМИ З РОЗПОДІЛЕНИМИ МОДУЛЯМИ ЕЛЕКТРОЕНЕРГЕТИЧНОЇ СИСТЕМИ

Космічна індустріалізація для освоєння нових ресурсів і середовищ існування є одним із перспективних напрямів сучасної аерокосмічної науки та техніки. Ключовою задачею є забезпечення промислової космічної платформи необхідною кількістю електроенергії. Одним із видів живлення таких модулів є використання розподілених систем, які складаються з угруповань космічних апаратів з безконтактною передачею електроенергії. Враховуючи це, постає проблема раціонального вибору орбіти для їх дислокації. Таким чином в роботі запропоновано методику вибору орбіт космічної промислової платформи та модулів розподіленої електроенергетичної системи. Ця методологія включає проведення оцінок орбітального поступального, кутового і відносного руху для кожного енергетичного космічного апарата, що є вхідними даними для розробленого алгоритму оптимального вибору орбіт. Алгоритм оптимізації включає статистичну обробку та елементи методів градієнтного і координатного спуску, що дозволяє визначити найбільш значущий параметр який впливає на тривалість сеансу безконтактної передачі електроенергії. Застосовано математику кватерніонів для оцінки динаміки зміни програмних параметрів наведення антени космічного апарата передавача на ректену космічного апарата приймача, що дає змогу визначити вимоги для системи керування кутовим рухом космічних енергетичних апаратів.

Використання запропонованої методології дозволяє сформувати вимоги для вибору відповідних проєктних параметрів системи керування розподіленою енергетичною системою космічної індустріальної платформи, а також проводити комплексне проєктування на концептуальних етапах розробки.

Ключові слова: безконтактна передача електроенергії; вибір орбіти; кватерніон націлювання; оптимізація параметрів орбіти.